JOURNAL OF GEOPHYSICAL RESEARCH: ATMOSPHERES, VOL. 118, 185–194, doi:10.1029/2012JD018464, 2013

Exploring parameterization for turbulent entrainment-mixing processes in clouds

Chunsong Lu,[1,2] Yangang Liu,[2] Shengjie Niu,[1] Steven Krueger,[3] and Timothy Wagner[4]

Received 11 July 2012; revised 29 November 2012; accepted 5 December 2012; published 16 January 2013.

[1] Different turbulent entrainment-mixing processes (e.g., homogeneous and inhomogeneous) occur in clouds; accurate representation of these processes is critical for improving cloud-related parameterizations in large-scale models, but poorly understood and quantified. Using in situ aircraft observations over the U. S. Department of Energy's Atmospheric Radiation Measurement Southern Great Plains site during the March 2000 Cloud Intensive Observation Period and numerical simulations with the Explicit Mixing Parcel Model (EMPM), here we explore the potential of using degree of homogeneous mixing as a measure to quantify these different mechanisms and examine various microphysical measures of homogeneous mixing degree and their relationships to entrainment-mixing dynamics as measured by transition scale numbers. Three different microphysical measures for the homogeneous mixing degree are newly defined and each is coupled with one of two different transition scale numbers. Both observations and simulations show that all the combinations have positive correlated relationships; simulations further show that the tightest relationship is between the measure of homogeneous mixing degree considering adiabatic number concentration and the transition scale number accounting for mixing fraction of dry air. A parameterization of the entrainment-mixing processes is advanced according to the relationships of homogeneous mixing degree measures to transition scale numbers.

Citation: Lu, C., Y. Liu, S. Niu, S. Krueger, and T. Wagner (2013), Exploring parameterization for turbulent entrainment-mixing processes in clouds, *J. Geophys. Res. Atmos.*, *118*, 185–194, doi:10.1029/2012JD018464.

1. Introduction

[2] Turbulent entrainment-mixing processes are critical to many outstanding issues related to clouds, including aerosol indirect effects, cloud-climate feedbacks, warm-rain initiation and remote sensing retrieval of cloud microphysical properties [*Paluch and Baumgardner*, 1989; *Yum*, 1998; *Ackerman et al*., 2004; *Kim et al*., 2008; *Del Genio and Wu*, 2010; *Lu et al*., 2011; *Kumar et al*., 2012; *Lu et al*., 2013]. Several different entrainment-mixing mechanisms have been proposed that may result in different cloud microphysical properties. Consider the homogeneous/inhomogeneous mixing model pioneered by *Baker and Latham* [1979] and *Baker et al*. [1980] for example. In the homogeneous mixing scenario, all droplets evaporate simultaneously; in the extreme inhomogeneous mixing scenario, some droplets evaporate completely while the rest of droplets do not evaporate at all. Although the conceptual model is well established, our understanding is still far from complete. Some observations suggested that the entrainment-mixing process was close to homogeneous [e.g., *Jensen et al*., 1985; *Burnet and Brenguier*, 2007; *Lehmann et al*., 2009]; others pointed to an inhomogeneous scenario [*Pawlowska et al*., 2000; *Burnet and Brenguier*, 2007; *Haman et al*., 2007; *Freud et al*., 2008, 2011; *Gerber et al*., 2008; *Lehmann et al*., 2009].

[3] The existence and our poor understanding of different types present a great challenge to accurate representation of entrainment-mixing processes and their various effects in atmospheric models. For example, *Lasher-Trapp et al*. [2005] found more large droplets were produced in a three-dimensional cloud model assuming inhomogeneous mixing than assuming homogeneous mixing. Using large eddy simulation, *Chosson et al*. [2007] found cloud albedo bias changed from −3% to −31% when assuming both mixing mechanisms alternatively in a fragmented and thin stratocumulus cloud. Similarly, with a cloud-resolving model, *Grabowski* [2006] found that the amount of solar energy reaching the surface was the same in the pristine case assuming the homogeneous mixing scenario as in the polluted case with the extreme inhomogeneous mixing; the same conclusion was also reported by *Slawinska et al*. [2008] using large eddy simulations with a one-moment microphysics scheme. Although later *Morrison and Grabowski* [2008], *Hill et al*. [2009], and

[1]CMA Key Laboratory for Aerosol-Cloud-Precipitation, Key Laboratory of Meteorological Disaster of Ministry of Education, Nanjing University of Information Science and Technology (NUIST), Nanjing, Jiangsu, China.
[2]Atmospheric Sciences Division, Brookhaven National Laboratory (BNL), Upton, New York, USA.
[3]Department of Meteorology, University of Utah, Salt Lake City, Utah, USA.
[4]Department of Atmospheric Sciences, Creighton University, Omaha, Nebraska, USA.

Corresponding author: C. Lu, Room 1117, Qixiang Bldg., No 219, Ningliu Rd., Pukou, Nanjing, Jiangsu, China. (luchunsong110@gmail.com)

2169-897X/13/2012JD018464

Slawinska et al. [2012] found significantly reduced effect of mixing mechanisms in simulations, *Morrison and Grabowski* [2008] and *Hill et al.* [2009] pointed out the effect of mixing mechanisms could be more significant over the entire cloud life cycle, especially during dissipation of clouds. Therefore, it is critical to distinguish homogeneous and inhomogeneous mixing. Furthermore, in real clouds, entrainment-mixing processes often fall between the above two extremes [*Andrejczuk et al.*, 2009; *Lu et al.*, 2011], posing an additional need for a quantitative measure that spans continuously over the two extreme types. This paper is motivated by such needs and focuses on examining the measure of homogeneous mixing degree, transition scale number [*Lu et al.*, 2011], and their relationships. Both in situ observations and numerical simulations are utilized in our analysis. A parameterization of turbulent entrainment-mixing process is advanced from the results.

[4] The rest of the paper is organized as follows. Section 2 defines three new measures of homogeneous mixing degree and describes the calculations of two transition scale numbers. Section 3 presents the results from in situ observations and numerical simulations. A summary is presented in section 4.

2. Homogeneous Mixing Degree and Transition Scale Number

2.1. Microphysical Measures of Homogeneous Mixing Degree

[5] The diagram of volume mean radius (r_v) versus number concentration (n), or its normalized version, r_v^3/r_{va}^3 versus n/n_a (r_{va} and n_a are adiabatic volume mean radius and number concentration, respectively) has been widely used to study homogeneous/inhomogeneous entrainment-mixing mechanisms [*Burnet and Brenguier*, 2007; *Lehmann et al.*, 2009; *Lu et al.*, 2011]. Based on the diagram of r_v^3/r_{va}^3 versus n/n_a, we can define three measures of homogeneous mixing degree.

[6] The first measure of homogenous mixing degree (ψ_1) is defined with the help of Figure 1a. Similar to Figure 5 in *Krueger* [2008], Figure 1a conceptually illustrates the sequence of states involved in an entrainment and isobaric mixing event. The states are numbered from 1 to 3. State 1 is an adiabatic cloud, which has adiabatic number concentration of n_a and volume mean radius of r_{va}. State 2 is just after entrainment but before evaporation, which has n_h and r_{va}. From States 2 to 3, mixing and evaporation occur; the number concentration and volume mean radius become n and r_v, respectively, after mixing and evaporation. The extreme inhomogeneous and homogeneous mixing scenarios are denoted by 3′ and 3″, respectively. The angle between the line linking States 2 and 3″ and the extreme inhomogeneous mixing line is π/2; the angle between the line linking States 2 and 3 and the extreme inhomogeneous mixing line is β. As an example, liquid water content is assumed to decrease to 0.2 of the adiabatic value.

[7] A trigonometrical analysis relates β to the slope of the line linking States 2 and 3:

$$\beta = \tan^{-1}\left(\frac{\frac{r_v^3}{r_{va}^3}-1}{\frac{n}{n_a}-\frac{n_h}{n_a}}\right), \tag{1}$$

[8] Normalizing β by π/2 gives the first measure of homogeneous mixing degree:

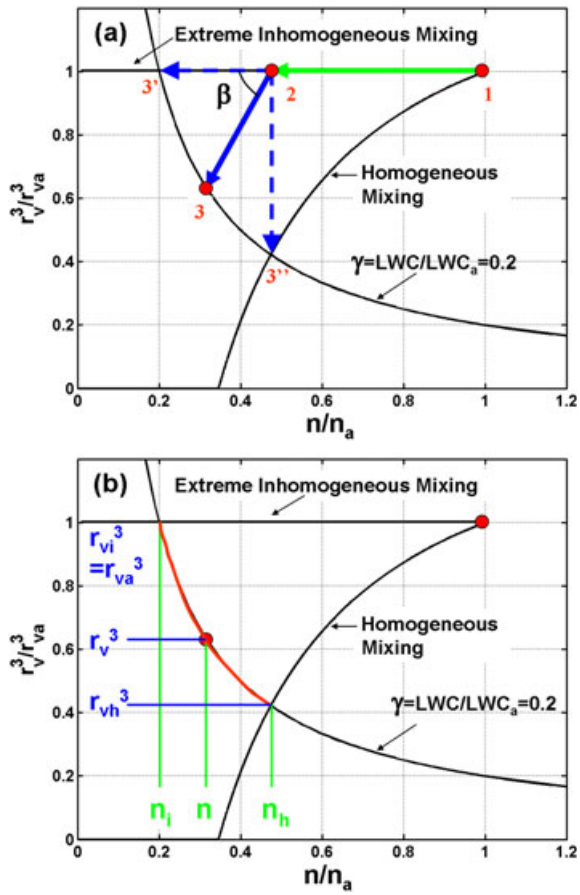

Figure 1. (a) Mixing diagram illustrating the definition of the first homogeneous mixing degree. The three black solid lines correspond to extreme inhomogeneous mixing, homogeneous mixing (relative humidity of the dry air is 66%), and contour of γ=0.2; γ is the ratio of liquid water content (LWC) to its adiabatic value (LWC_a). See text for the meanings of the other lines and symbols. (b) Same as Figure 1a but for the definition of the second and third homogeneous mixing degree.

$$\psi_1 = \frac{\beta}{\pi/2} \tag{2}$$

[9] Obviously, ψ_1 is between 0 and 1 and measures the degree of homogeneous mixing: a larger ψ_1 indicates a higher degree of homogeneous mixing, with $\psi_1=1$ for homogeneous mixing and $\psi_1=0$ for extreme inhomogeneous mixing.

[10] The second measure of homogeneous mixing degree (ψ_2) is illustrated with Figure 1b. When a mixing process is homogeneous, the number concentration and volume mean radius are n_h and r_{vh}, respectively; when a mixing process is extreme inhomogeneous, the number concentration and volume mean radius are n_i and r_{va}, respectively. In reality, the mixing scenario is between the two extremes with number concentration of n and volume mean radius of r_v. The second measure of homogeneous mixing degree is expressed as

$$\psi_2 = \frac{1}{2}\left(\frac{n-n_i}{n_h-n_i} + \frac{r_v^3-r_{va}^3}{r_{vh}^3-r_{va}^3}\right), \quad (3)$$

where

$$r_{vh}^3 = \frac{n}{n_h} r_v^3, \quad (4)$$

$$n_i = \frac{r_v^3}{r_{va}^3} n. \quad (5)$$

[11] The third measure of homogeneous mixing degree (ψ_3) can be defined by recognizing that the logarithm operation linearizes the nonlinear ${r_v}^3/{r_{va}}^3 - n/n_a$ relation such that

$$\psi_3 = \frac{\ln n - \ln n_i}{\ln n_h - \ln n_i} = \frac{\ln r_v^3 - \ln r_{va}^3}{\ln r_{vh}^3 - \ln r_{va}^3}. \quad (6)$$

[12] In a numerical study, *Morrison and Grabowski* [2008] introduced an empirical parameter to quantify the homogeneous mixing degree such that

$$n = n_0 \left(\frac{q_L}{q_{L0}}\right)^{\alpha}, \quad (7)$$

where n_0 and q_{L0} are number concentration and liquid water mixing ratio after entrainment but before evaporation, respectively; n_0 is identical to n_h in equation (3); n and q_L are final number concentration and liquid water mixing ratio, respectively, after mixing and evaporation. These two properties are taken as the values after new saturation is achieved. It can be shown that ψ_3 is uniquely related to α by

$$\psi_3 = 1 - \alpha, \quad (8)$$

[13] Note that *Morrison and Grabowski* [2008] prescribed three α values (=0, 0.5, and 1) in their simulations, instead of examining the link between α and microphysical relationships.

2.2. Transition Scale Numbers

[14] The transition scale number (N_L) is a dynamical measure of the occurrence probability of homogeneous or inhomogeneous entrainment-mixing process [*Lu et al.*, 2011]; the larger the N_L, the stronger the homogenous entrainment-mixing process and the weaker the inhomogeneous entrainment-mixing process. N_L is calculated as the ratio of transition length (L^*) introduced by *Lehmann et al.* [2009] to the Kolmogorov microscale (η):

$$N_L = \frac{L^*}{\eta} = \frac{\varepsilon^{1/2}\tau_{\text{react}}^{3/2}}{\eta}, \quad (9)$$

where ε is eddy dissipation rate. η is given by

$$\eta = \left(\frac{V^3}{\varepsilon}\right)^{1/4} \quad (10)$$

where v is the kinematic viscosity [*Wyngaard*, 2010]. The reaction time τ_{react} is the time when droplets have completely evaporated or relative humidity has reached 99.5% ($s > -0.005$) [*Lehmann et al.*, 2009] whichever is first satisfied; it is calculated by the following equations:

$$\frac{dr}{dt} = A\frac{s}{r}, \quad (11a)$$

$$\frac{ds}{dt} = -Brs, \quad (11b)$$

where r is cloud droplet radius, s supersaturation, A a function of pressure and temperature, and B a function of pressure and temperature and proportional to cloud droplet number concentration [*Rogers and Yau*, 1989]. If n_a is used in B, scale number is denoted by N_{La}; while if n_0 is used, scale number is denoted by N_{L0}. For a group of droplets, r in the above equations is replaced with r_{va}.

3. Relationship between Homogeneous Mixing Degree and Transition Scale Number

[15] Although a positive relationship between the microphysical measures of homogeneous mixing degree and transition scale number is expected from the fact that the two measures quantify the probability of the homogeneous mixing process from different perspectives, the details of the relationship remain elusive. Next we explore this relationship by examining both in situ cloud observations and numerical simulations.

3.1. Observational Results

[16] The stratocumulus clouds were collected over the U. S. Department of Energy's Atmospheric Radiation Measurement Southern Great Plains site during the March 2000 Cloud Intensive Observation Period (IOP). Cloud droplet and drizzle size distributions were measured with a Particle Measuring Systems (PMS) Forward Scattering Spectrometer Probe (FSSP-100) and an optical array probe (1D-C), respectively. The FSSP probe sizes and counts cloud droplets in 15 bins, with bin centers from 2.7 to 30 μm radius; the 1D-C probe has 30 bins with bin centers from 12.1 to 300 μm radius. Measurements of both instruments are corrected with standard procedures [*Dye and Baumgardner*, 1984; *Baumgardner et al.*, 1985; *Baumgardner*, 1987; *Baumgardner and Spowart*, 1990]. Air temperature, air pressure, and dew point were measured with Rosemount Model 102, Rosemount Model 1201F1, and EG&G Model 137 probes, respectively. Relative humidity is calculated based on the dew point, air temperature, and air pressure. True air speed was measured by Rosemount 1221F. The turbulence dissipation rate is derived from the true airspeed using a structure function (see Appendix A in *Lu et al.* [2011] for details). The 1 Hz data are used in this study.

[17] Sixteen non-drizzling horizontal flight legs in five flights were used to study homogeneous/inhomogeneous mixing with the relationship of $r_v - n$ by *Lu et al.* [2011]. One leg was affected by homogeneous mixing, 13 were affected by extreme inhomogeneous mixing, and two were affected by inhomogeneous mixing with subsequent ascent. In the definitions of ψ_1, ψ_2, and ψ_3, subsequent ascent after the mixing process is not considered, so the legs, except the two legs affected by inhomogeneous mixing with subsequent ascent, are used here.

[18] To obtain the properties used in the calculations of ψ_1, ψ_2, ψ_3, N_{La}, and N_{L0}, mixing fraction of dry air (f) for each of the 14 legs is needed and can be calculated based

on the equations [*Burnet and Brenguier*, 2007; *Gerber et al*., 2008; *Lehmann et al*., 2009]:

$$q_L + q_{vs}(T) = [q_{vs}(T_a) + q_{La}](1-f) + q_{ve}f, \quad (12a)$$

$$c_pT = c_pT_a(1-f) + c_pT_ef - L_v[q_{La}(1-f) - q_L], \quad (12b)$$

$$q_{vs}(T) = 0.622\frac{e_s(T)}{p - e_s(T)}, \quad (12c)$$

where T, $q_{vs}(T)$, and q_L are, respectively, the average temperature, saturation vapor mixing ratio, and liquid water mixing ratio along each leg; T_e and q_{ve} are, respectively, temperature and water vapor mixing ratio of the entrained dry air from above the cloud tops; e_s is saturation vapor pressure; c_p is specific heat capacity at constant pressure; p is air pressure; L_v is latent heat; T_a, $q_{vs}(T_a)$, and q_{La} are, respectively, the temperature, saturation vapor mixing ratio, and liquid water mixing ratio in the adiabatic cloud parcel. The maximum liquid water mixing ratio along a leg is assumed to be q_{La}; the temperature corresponding to q_{La} is assumed to be T_a. Then f along the horizontal legs is calculated with the input parameters q_{La}, T_a, q_L, T_e, and q_{ve} (Table 1). With f and assuming the maximum number concentration along a leg is n_a, n_h can be calculated with $n_h = n_a(1-f)$. The average number concentration along a leg is taken to be n. Thus, r_v is given by

$$r_v = \left(\frac{q_L\rho_{\text{air}}}{4/3\pi n\rho}\right)^{1/3} \quad (13)$$

where ρ and ρ_{air} are water density and air density, respectively. Similarly, r_{va} is calculated with q_{La} and n_a. Then r_{vh} and n_i are calculated by equations (4) and (5), respectively.

[19] With all the above properties, ψ_1, ψ_2, ψ_3, N_{La}, and N_{L0} can be calculated and the results are shown in Figure 2. The positive correlations between ψ_1, ψ_2, ψ_3 and N_{La}, N_{L0} are evident for 12 out of 14 legs, but with large scatter. One reason for the scatter of data points is the influence of dissipation rate, relative humidity, adiabatic number concentration, and mixing fraction of dry air, which will be discussed later; another reason could be the uncertainties of obtaining the quantities needed in equations (1)–(11b) from observations. Also note that ψ_1, ψ_2, and ψ_3 along the other two legs are negative, which cannot be shown in the logarithmic space. The reason for the negative values is that n along each of these two legs is smaller than n_i, which may be related to the uncertainties of the cloud properties determined from observations, such as n_a. *Freud et al*. [2011] pointed out that n_a determined by observed maximum number concentration may be sensitive to small-scale processes (e.g., local strong updraft near cloud base, since n_a is sensitive to updraft [e.g., *Lu et al*., 2012a]) and be affected by the extent of dilution that the measured cloud has experienced; they developed a new approach to estimate n_a but this approach is not applicable to the stratocumulus clouds in this study, because applying this approach requires penetrations at different levels in convective clouds. Fortunately, these two legs with negative homogeneous mixing degrees have small N_{La} and N_{L0} (<10) and the data points for these legs would be located in the bottom left corner if Figure 2 was plotted in the linear space, still supporting the positive relationships of ψ_1, ψ_2, ψ_3 to N_{La}, N_{L0}. Also note that the values of neither N_{La} nor N_{L0} are equal to the scale numbers used in *Lu et al*. [2011]; the reason is that the number concentration and mean radius used in *Lu et al*. [2011] were instantaneous values observed by aircraft at 1 Hz; after instantaneous scale number was calculated, the values were averaged to the leg-averaged scale number. This is different from the calculations of N_{La} and N_{L0}. For example, the number concentration and droplet size used to calculate N_{La} are adiabatic number concentration and adiabatic volume mean radius, respectively.

3.2. Numerical Results

[20] As discussed above, some properties (e.g., n_a) determined from observations have uncertainties that affect the calculations of ψ_1, ψ_2, ψ_3, N_{La}, and N_{L0}, and thus their relationships. To further examine the relationships in detail, the Explicit Mixing Parcel Model (EMPM) is employed.

3.2.1. Model Description and Simulation Parameters

[21] The EMPM was developed by *Krueger et al*. [1997]; *Su et al*. [1998] further included individual droplet growth in the model. The model depicts the fine-scale internal structure of a rising parcel using a 1D domain. The internal

Table 1. General Characteristics Above Cloud Tops and Along Horizontal Aircraft Legs in Stratocumulus During the 2000 Cloud Intensive Observation Period

Case	Leg	T_e (K)	RH_e (%)	p (hPa)	q_{La} (gkg^{-1})	T_a (K)	n_a (cm^{-3})	r_{va} (μm)	q_L (gkg^{-1})	n (cm^{-3})	r_v (μm)	f
03 March 2000	1	273.6	0.61	879.2	0.61	270.8	470.6	7.1	0.28	240.9	7.5	0.21
03 March 2000	2	273.6	0.61	882.8	0.39	271.0	501.3	6.0	0.23	330.9	6.2	0.12
03 March 2000	3	273.6	0.61	889.8	0.48	271.5	491.1	6.4	0.20	270.4	6.2	0.19
03 March 2000	5	273.6	0.61	849.1	0.62	269.6	403.0	7.4	0.35	245.6	7.4	0.16
17 March 2000	1	268.1	0.62	850.2	0.19	277.0	89.4	8.2	0.13	55.3	8.4	0.14
17 March 2000	2	268.1	0.62	913.9	0.61	274.2	331.0	8.0	0.30	205.3	7.6	0.27
19 March 2000	1	275.4	0.42	877.6	0.56	271.0	443.9	7.0	0.21	190.4	7.3	0.16
19 March 2000	2	275.4	0.42	893.9	0.36	272.0	489.1	5.9	0.15	215.8	5.8	0.11
19 March 2000	3	275.4	0.42	900.2	0.41	272.1	640.8	5.6	0.16	240.1	5.6	0.12
19 March 2000	4	275.4	0.42	893.3	0.39	273.5	531.5	5.8	0.14	250.5	5.5	0.13
19 March 2000	5	275.4	0.42	886.7	0.40	273.3	489.0	6.0	0.19	278.8	5.7	0.11
19 March 2000	6	275.4	0.42	896.5	0.34	273.0	545.5	5.6	0.15	270.0	5.4	0.10
19 March 2000	7	275.4	0.42	906.7	0.31	273.5	537.9	5.4	0.13	287.5	5.0	0.10
21 March 2000	1	272.2	0.27	728.2	1.03	275.8	204.5	10.3	0.49	102.7	10.6	0.20

[a]With air temperature T_e and relative humidity RH_e above the cloud tops, air pressure p, adiabatic liquid water mixing ratio q_{La}, temperature T_a corresponding to q_{La}, adiabatic droplet number concentration n_a, adiabatic volume mean radius r_{va}, average liquid water mixing ratio q_L, average droplet number concentration n, average volume mean radius r_v, and mixing fraction of dry air f along different horizontal legs.

[b]The leg numbers are the same as those in Figure 1 in *Lu et al*. [2011].

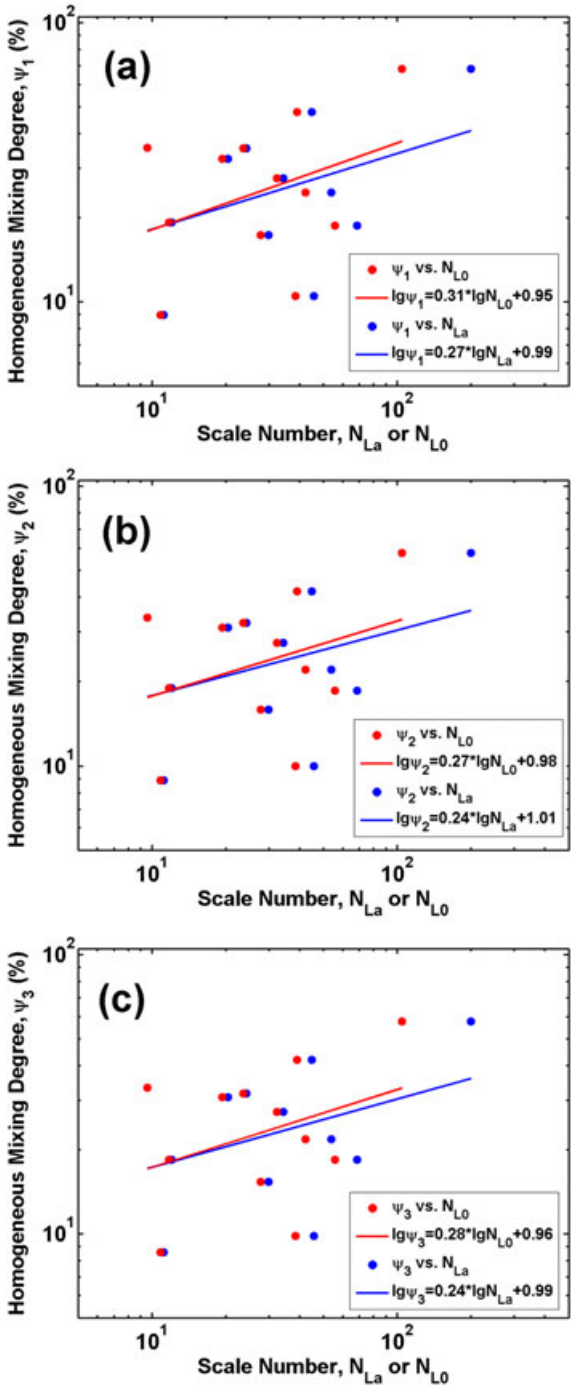

Figure 2. Observational relationships between the (a–c) three measures of homogeneous mixing degree (ψ_1, ψ_2, ψ_3) and the two scale numbers (N_{La}, N_{L0}), respectively, along 12 horizontal aircraft legs in stratocumulus clouds observed during the March 2000 Cloud Intensive Observation Period. Two legs with negative homogeneous mixing degree are not shown in the logarithmic space. See text for the details.

structure evolves in the model as a consequence of discrete entrainment events and explicit turbulent mixing based on the linear eddy model developed by *Kerstein* [1988; 1992]. As summarized by *Krueger* [2008], the model works as follows. First, the parcel ascends adiabatically above cloud base, while the droplets grow by condensation. Second, when entrainment occurs, the subsaturated entrained air replaces a same-sized segment of the cloudy parcel. Third, the cloudy air and the newly entrained air undergo a finite rate turbulent isobaric mixing process, during which many droplets encounter the entrained subsaturated air, resulting in partial or even total evaporation of some droplets.

[22] Table 2 summarizes the input parameters of the model. In this study, the cloud base and environmental information are taken from Hawaiian trade cumulus cloud measurements [*Raga et al.*, 1990]. The cloud base pressure, temperature, and water vapor mixing ratio are 964.0 hPa, 293.6K, and 15.7 g kg^{-1}, respectively. The n_a is 102.7 cm^{-3}; these droplets are randomly assigned to the 20 m (width) × 0.001 m (height) × 0.001 m (depth) model domain. The entrainment level is set at the pressure of 888.9 hPa where the temperature and relative humidity in the entrained air are 289.3K and 88%, respectively. Updraft is set to be a constant, 2 m s^{-1}, before the entrainment level; after that the parcel stops rising and isobaric mixing occurs. The grid size is set to be 0.0017 m × 0.001 m × 0.001 m. The time step of model output is 0.75 s.

[23] To explore the relationship between the homogeneous mixing degree and the transition scale number, we perform a suite of simulations with different combinations of model parameters: n_a is set to be 102.7, 205.4, 308.1, 410.8, and 513.5 cm^{-3}; relative humidity (RH) is set to be 11%, 22%, 44%, 66%, and 88%; ε is set to be 1×10^{-5}, 5×10^{-4}, 1×10^{-3}, 5×10^{-3}, 1×10^{-2}, and 5×10^{-2} m^2 s^{-3}; blob number is set to be 2–9 and the entrained blob size is 2 m × 0.001 m × 0.001 m; so mixing fraction of dry air is 0.2–0.9. When the blob number is 1, the mixing fraction of dry air is small and most of the domain is occupied by adiabatic cloud. In the adiabatic cloud, droplet size increases due to residual supersaturation. As a result, r_v over the domain increases, especially for higher RH. To minimize this effect and focus on the entrainment-mixing processes, the blob number starts from 2.

3.2.2. Results from EMPM

[24] Figure 3 compares the relationships of homogeneous mixing degree measures (ψ_1, ψ_2, ψ_3) to the transition scale numbers (N_{La}, N_{L0}). In every entrainment and isobaric mixing process, liquid water mixing ratio decreases sharply. When the liquid water mixing ratio stops decreasing for a 5 s period, it is assumed that a new saturation level is achieved; the n and r_v in the domain are considered to be the final values used in the calculations of ψ_1, ψ_2, and ψ_3. The values of ψ_1, ψ_2, and ψ_3 are not sensitive to the waiting period of "5 s." Investigations of ψ_1 with a waiting period of 3 s and 10 s have relative differences of 0.5–1% when compared to the control of 5 s. In some sensitivity tests, clouds completely evaporate due to the large mixing fraction of dry air and/or low relative humidity (e.g., mixing fraction of dry air from 0.3 to 0.9, RH=11%); these cases are not included in Figure 3. Positive relationships between the three measures of homogeneous mixing degree and the scale numbers are found in two regimes: RH=11%, 22%, 44%, and 66% and RH=88%. The reason for the two regimes is that different conditions are satisfied in solving equations (11a) and (11b) to obtain τ_{react} and then N_L; for RH=11%, 22%, 44%, and 66% and for RH=88%, the first condition "droplets have completely evaporated" and the second condition "relative humidity has reached 99.5%" are satisfied, respectively. For RH=88%,

Table 2. Input Parameters for the EMPM

	Parameters	Values
Cloud base conditions	Cloud base pressure (hPa)	964.0
	Cloud base temperature (K)	293.6
	Cloud base water vapor mixing ratio (gkg^{-3})	15.7
	Adiabatic droplet number concentration, n_a (cm^{-3})	102.7, 205.4, 308.1, 410.8, 513.5
Entrainment conditions	Domain size (m)	$20\times0.001\times0.001$
	Entrainment level pressure (hPa)	888.9
	Entrained air temperature (K)	289.3
	Entrained air relative humidity, RH (%)	11, 22, 44, 66, 88
	Vertical velocity	Before mixing $2ms^{-1}$, after mixing $0ms^{-1}$.
	Grid size (m)	0.0017
	Dissipation rate, ε (m^2s^{-3})	1×10^{-5}, 5×10^{-4}, 1×10^{-3}, 5×10^{-3}, 1×10^{-2}, 5×10^{-2}
	Entrained air blob size (m^3)	$2\times0.001\times0.001$
	Entrained air blob number	2, 3, 4, 5, 6, 7, 8, 9
	Mixing fraction of dry air, f	0.2, 0.3, 0.4, 0.5, 0.6, 0.7, 0.8, 0.9

most of ψ_1, ψ_2, and ψ_3 are close to 100%; it is less important to distinguish homogeneous and inhomogeneous mixing when entrained dry air has a high relative humidity since evaporation is relatively small [*Lehmann et al*., 2009; *Devenish et al*., 2012; *Slawinska et al*., 2012]. Only when mixing fraction of dry air is large, it becomes important to distinguish mixing types; for example, as shown in Figure 3b, some green and black points (RH=88%) with f=0.5 have ψ_2 around 70%. This is supported by Figure 1 in *Freud et al*. [2011], where the homogeneous mixing line for RH=90% is close to the extreme inhomogeneous mixing line when adiabatic fraction (the ratio of liquid water content to its adiabatic value) is larger than 0.4; only when adiabatic fraction becomes smaller (i.e., mixing fraction of dry air becomes larger), e.g., 0.2, the homogeneous mixing line deviates quite remarkably from the extreme inhomogeneous mixing line. Here we will focus on the regime with RH=11%, 22%, 44%, and 66%; the best fitting lines are also shown in Figure 3.

[25] As shown in Figure 3, ψ_2 versus N_L and ψ_3 versus N_L are close to each other, while ψ_1 versus N_L has the tightest relationship. To be clearer, Figure 4 shows that ψ_2 and ψ_3 are close to each other, and ψ_1 has larger values than ψ_2 (and ψ_3). Since the upper limit of ψ_1, ψ_2, and ψ_3 is 100%, ψ_1 has a smaller range than ψ_2 and ψ_3, and ψ_1 versus N_L is the tightest. The physical reason for the tightest ψ_1 versus N_L may be that the calculation of ψ_1 needs one more constraint (i.e., n_a) than ψ_2 and ψ_3 [equations (1)–(8)]. A tight relationship is important for a parameterization; thus it is suggested to use ψ_1 if n_a is available [n_a is necessary in equation (1)], otherwise, use ψ_2 or ψ_3. Figure 3 also shows that the relationships of ψ_1, ψ_2, and ψ_3 to N_{L0} are tighter than those of ψ_1, ψ_2, and ψ_3 to N_{La}, which is especially true for ψ_2 and ψ_3. To figure out the reasons, Figure 5 compares ψ_3 versus N_{La} and ψ_3 versus N_{L0} with a mixing fraction of dry air changing from 0.2 to 0.5; others being equal, the ψ_3 is smaller with a larger mixing fraction of dry air; for example, ψ_3 decreases from "1" to "2" or from "I" to "II." This is consistent with observations in cumuli analyzed by *Burnet and Brenguier* [2007]; they found that mixing approached the homogeneous type when mixing fraction of dry air was small and approached the inhomogeneous type when mixing fraction of dry air was large. Similar conclusion can also be drawn from Figures 5a and 5b in *Lehmann et al*. [2009]. Other studies have also proven that mixing fraction of dry air is critical for mixing processes [*Jensen and Baker*, 1989; *Hicks et al*., 1990; *Schlüter*, 2006; *Jeffery*, 2007]. N_{La} cannot reflect the role of dry air mixing fraction but N_{L0} can. The reason is in the calculation of N_{La}, the number concentration used in the calculation of B in equations (11a) and (11b) is the adiabatic number concentration which is independent of mixing fraction; as for N_{L0}, the number concentration used is the number concentration just after entrainment, which considers the mixing fraction. As a result, the change from "I" to "II" is along a vertical line while that from "1" to "2" is toward the bottom left corner of Figure 5; thus the relationship of ψ_3 versus N_{Lo} (the red points and squares) is tighter than that of ψ_3 versus N_{La} (the green points and squares). Thus it is suggested to use N_{L0} instead of N_{La} in the future studies.

[26] Although the relationships are tighter with N_{L0}, dispersion of the data points in Figure 3 still exists. To further determine the influencing factors, the effects of dissipation rate, relative humidity, adiabatic number concentration, and mixing fraction of dry air are examined. As exemplified in Figure 6, in every group (e.g., "ψ_1 versus N_{L0}, RH=11%" in Figure 6a), the dissipation rates of the six data points from left to right are 1×10^{-5}, 5×10^{-4}, 1×10^{-3}, 5×10^{-3}, 1×10^{-2}, and $5\times10^{-2}m^2s^{-3}$, respectively. Smaller dissipation rates correspond to smaller homogeneous mixing degree values, because a smaller dissipation rate means a slower mixing process, which is favorable for inhomogeneous mixing process [e.g., *Baker et al*., 1984]. Comparison of the results with RH=66% and 11% shows that lower RH causes smaller ψ and a larger slope of ψ versus N_{L0} (Figure 6a); lower RH means faster evaporation of droplets, making mixing more likely inhomogeneous [e.g., *Siebert et al*., 2006]. Figure 6b shows that ψ is smaller for a larger adiabatic droplet number concentration, because a larger adiabatic number concentration causes smaller droplets, increasing the likelihoods of complete evaporation and extreme inhomogeneous mixing [e.g., *Hill et al*., 2009]. As discussed above, larger mixing fraction of dry air causes more inhomogeneous mixing, i.e., smaller ψ (Figures 5 and 6c). These factors altogether affect the relationships between the homogeneous mixing degree and the scale number.

[27] In addition, the combination of N_{L0} and a new approach for estimating entrainment rate (λ) [*Lu et al*., 2012b, 2012c] presents a potential to link the two sides of entrainment-mixing processes, i.e., entrainment rate and

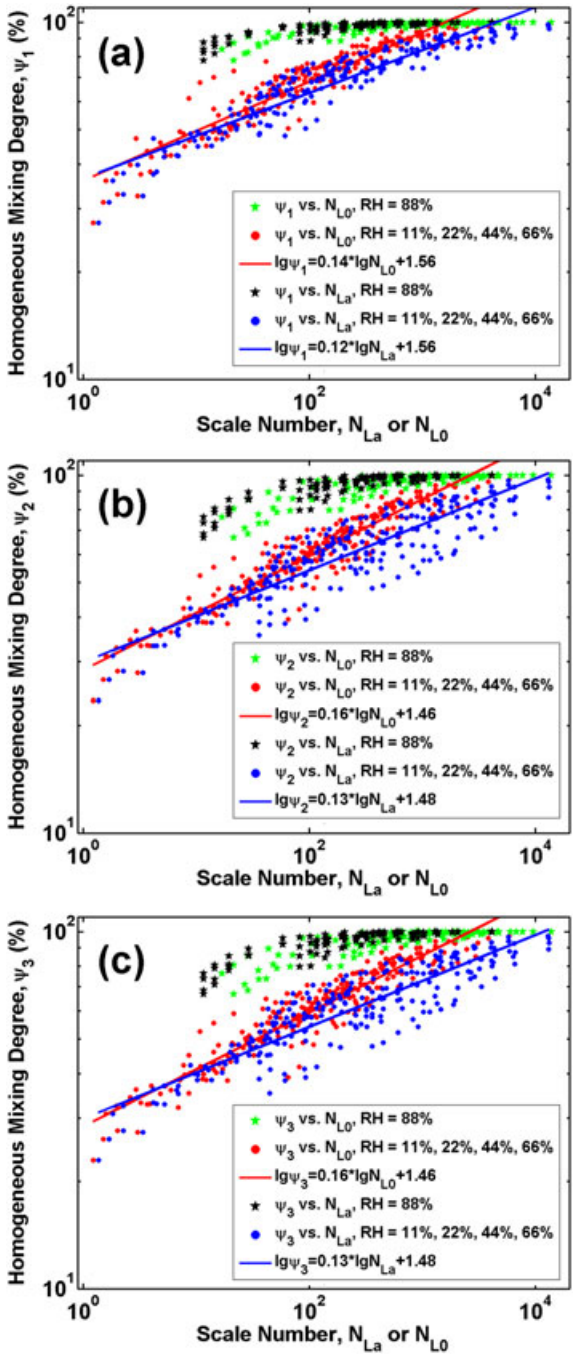

Figure 3. The relationships between the (a–c) three measures of homogeneous mixing degree (ψ_1, ψ_2, ψ_3) and the two scale numbers (N_{La}, N_{L0}), respectively, under all kinds of conditions as listed in Table 2 except the cases where clouds completely dissipate.

the entrainment-mixing mechanisms. This new approach is directly derived from the definition of λ and relates it to f and the height above cloud base (h).

$$\lambda = -\frac{\ln(1-f)}{h} \tag{14}$$

[28] Since in the current simulation, the model domain does not move upward during mixing, so h is fixed for

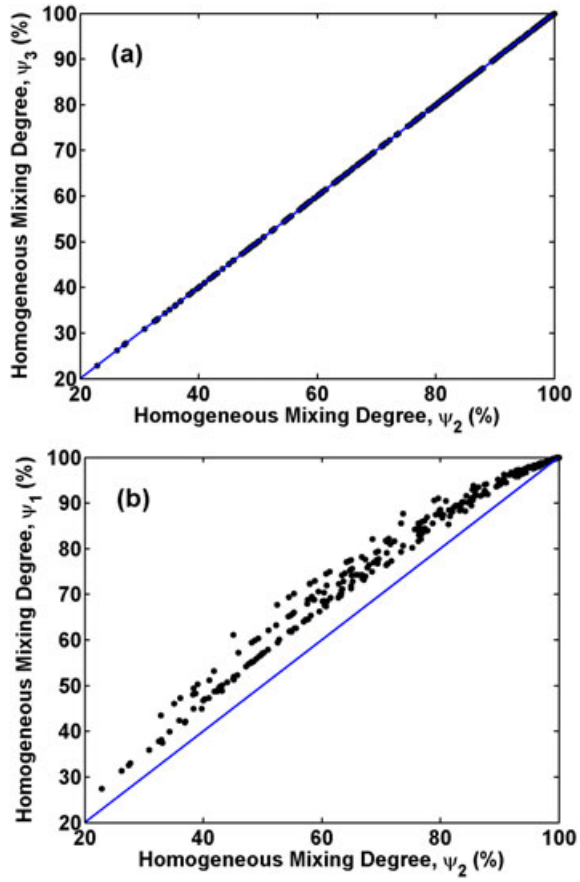

Figure 4. (a) The relationship between the third homogeneous mixing degree (ψ_3) and the second homogeneous mixing degree (ψ_2); (b) the relationship between the first homogeneous mixing degree (ψ_1) and ψ_2.

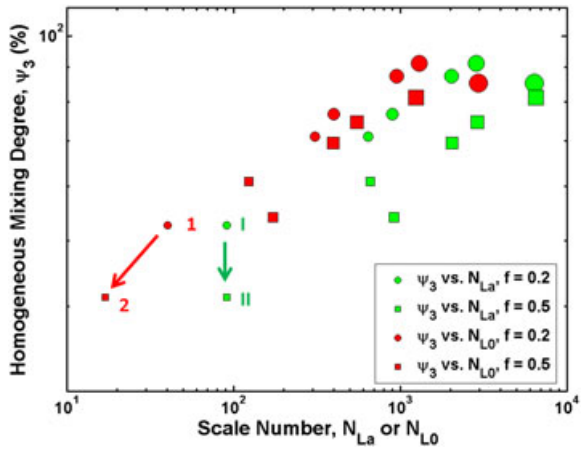

Figure 5. The relationships between the homogeneous mixing degree (ψ_3) and the two scale numbers (N_{La}, N_{L0}), respectively, with two mixing fractions of dry air (f) being 0.2 and 0.5. The relative humidity (RH) and adiabatic number concentration (n_a) are 66% and 205.4 cm^{-3}, respectively; in every group (e.g., ψ_3 versus N_{La}, f=0.2), dissipation rates are 1×10^{-5}, 5×10^{-4}, 1×10^{-3}, 5×10^{-3}, 1×10^{-2}, and 5×10^{-2} m^2s^{-3} for the six data points (from left to right and from small to big size), respectively.

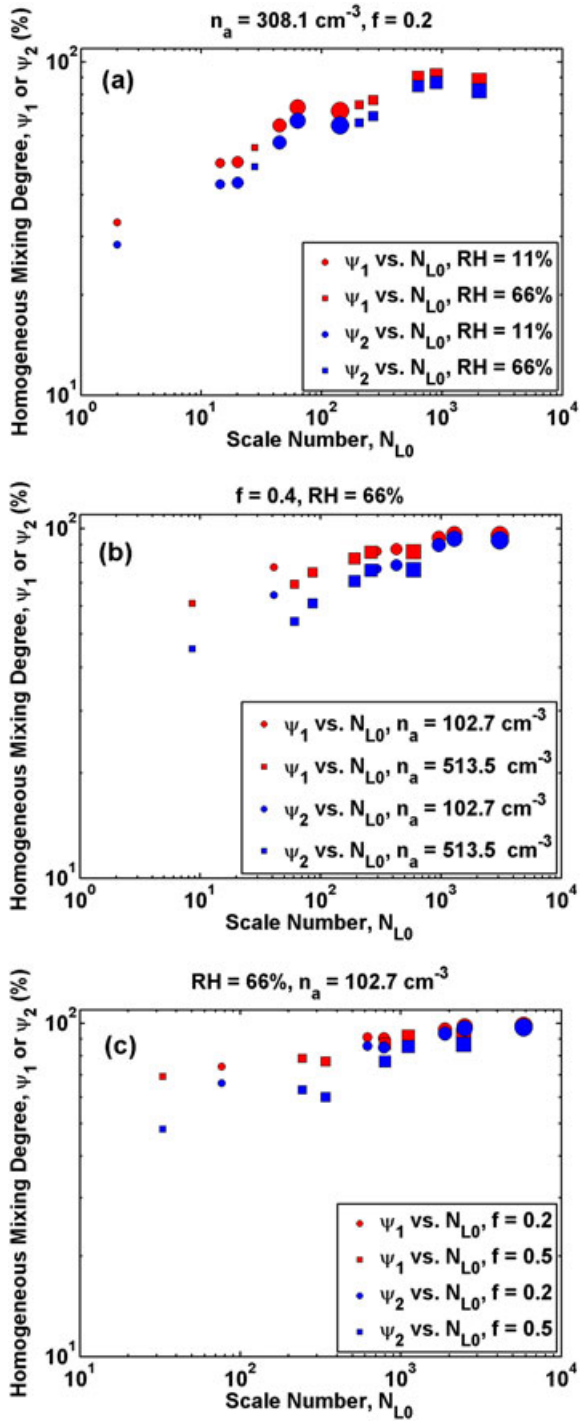

Figure 6. (a) Relationships between two measures of homogeneous mixing degree (ψ_1, ψ_2) and the scale number (N_{L0}), respectively, with relative humidity (RH) being 11% and 66%; adiabatic number concentration (n_a) and mixing fraction of dry air (f) are 308.1 cm^{-3} and 0.2, respectively. (b) Relationships between ψ_1, ψ_2, and N_{L0}, respectively, with n_a being 102.7 and 513.5 cm^{-3}; f and RH are 0.4 and 66%, respectively. (c) Relationships between ψ_1, ψ_2, and N_{L0}, respectively, with f being 0.2 and 0.5; RH and n_a are 66% and 102.7 cm^{-3}, respectively. In every group (e.g., ψ_1 versus N_{L0}, RH=11%), dissipation rates are 1×10^{-5}, 5×10^{-4}, 1×10^{-3}, 5×10^{-3}, 1×10^{-2}, and 5×10^{-2} m^{2}s^{-3} for the six data points (from left to right and from small to big size), respectively.

different simulations and λ is determined only by f. Since λ increases with increasing f, the effect of λ on the relationship of ψ versus N_L (not shown) is similar to the effect of f as shown in Figure 6c. Future study will go beyond single isobaric mixing event since the EMPM and the new approach are applicable for multiple mixing events at different heights, which is believed to provide more insights on the link between the two sides of entrainment-mixing processes.

4. Summary

[29] The relationship between the homogeneous mixing degree and the transition scale number is examined with in situ cloud observations over the U.S. Department of Energy's Atmospheric Radiation Measurement Southern Great Plains site during the March 2000 Cloud Intensive Observation Period and numerical simulations using the Explicit Mixing Parcel Model. Three measures of homogeneous mixing degree are newly defined and two transition scale numbers are used. As theoretically expected, the three homogeneous mixing degrees are all positively related to the two scale numbers based on both the observations and simulations. Numerical simulations further show that among the three measures of homogeneous mixing degree, it is suggested to use the first homogeneous mixing degree (ψ_1) if adiabatic number concentration (n_a) is available, because ψ_1 has the tightest relationship with the two scale numbers; otherwise, use the second or third homogeneous mixing degree (ψ_2 or ψ_3) instead. As to transition scale numbers, it is suggested to use N_{L0} instead of N_{La} in the future studies of entrainment-mixing processes because the relationships of N_{L0} to the three homogeneous mixing degree measures are tighter than the relationships of N_{La} to the three measures. The reason is that N_{L0} considers mixing fraction of dry air while N_{La} does not. Besides this advantage of N_{L0}, the combination of N_{L0} and a new entrainment rate estimation approach [*Lu et al.*, 2012c] presents a potential to link the two sides of entrainment-mixing processes (homogeneous/inhomogeneous entrainment-mixing mechanisms and entrainment rate).

[30] The relationship between the homogeneous mixing degree and transition scale number also suggests a new parameterization for entrainment-mixing processes in models with two-moment microphysical schemes. The transition scale number can be calculated from the microphysical properties [volume mean radius (r_{va}) and adiabatic number concentration (n_a) or number concentration just after dilution (n_0)] and meteorological elements before mixing and evaporation for every cloud grid at every time step in models; the degree of homogeneous mixing can be estimated from the transition scale number based on the best fitting lines in Figure 3; with the homogeneous mixing degree and equations (2), (3), or (6), the values of number concentration (n) and volume mean radius (r_v) after the mixing and evaporation can be calculated.

[31] Three points are noteworthy. First, the relationship between the microphysical homogeneous mixing degree and transition scale number is obtained from in situ observations and numerical simulations in this study. Further theoretical exploration is needed to improve our understanding and quantification of the relationship. Second, all isobaric mixing events in this study are assumed to be between an adiabatic parcel and dry air. This assumption may make the mixing look more homogeneous than reality as secondary mixing events

may start with droplets smaller than the droplets in an adiabatic parcel. In future work, we will decrease the size of one dry blob and assume that the number of entraining dry air blobs during multiple successive entrainment events can be described by a stochastic function, such as a Gaussian distribution, since entrainment mixing is a stochastic process [*Romps and Kuang*, 2010]. Thus the effect of secondary mixing may be examined in detail. Third, the evolution of droplet size distributions during entrainment mixing processes should be further studied, because the $r_v - n$ relationship has its own limitation. Even in fully homogeneous mixing, the smallest droplets may fully evaporate and n may be smaller than the number concentration during homogeneous mixing (n_h); as a result, r_v may be slightly larger than volume mean radius during homogeneous mixing (r_{vh}) [*Freud et al.*, 2011].

[32] **Acknowledgments.** We thank Satoshi Endo at the Brookhaven National Lab for many useful discussions on this manuscript. This research is supported by open funding (No. KDW1201) from CMA Key Laboratory for Aerosol-Cloud-Precipitation in the Nanjing University of Information Science and Technology, Jiangsu, China (Lu), by the Qing-Lan Project for Cloud-Fog-Precipitation-Aerosol Study in Jiangsu Province, China, a Project Funded by the Priority Academic Program Development of Jiangsu Higher Education Institutions (Lu and Niu), and by the U.S. Department of Energy's (DOE) Earth System Modeling (ESM) program via the FASTER project (www.bnl.gov/esm) and Atmospheric System Research (ASR) program (Lu and Liu). The development of the EMPM was supported by the Office of Naval Research under grant N00014-91-J-1175.

References

Ackerman, A. S., M. P. Kirkpatrick, D. E. Stevens, and O. B. Toon (2004), The impact of humidity above stratiform clouds on indirect aerosol climate forcing, *Nature*, *432*(7020), 1014-1017.

Andrejczuk, M., W. W. Grabowski, S. P. Malinowski, and P. K. Smolarkiewicz (2009), Numerical simulation of cloud–clear air interfacial mixing: Homogeneous versus inhomogeneous mixing, *J. Atmos. Sci.*, *66*(8), 2493–2500, doi:10.1175/2009JAS2956.1.

Baker, M. B., and J. Latham (1979), The evolution of droplet spectra and the rate of production of embryonic raindrops in small cumulus clouds, *J. Atmos. Sci.*, *36*(8), 1612-1615, doi:10.1175/1520-0469(1979)036<1612:TEODSA>2.0.CO;2.

Baker, M. B., R. G. Corbin, and J. Latham (1980), The influence of entrainment on the evolution of cloud droplet spectra: I. A model of inhomogeneous mixing, *Q. J. Roy. Meteor. Soc.*, *106*(449), 581–598, doi:10.1002/qj.49710644914.

Baker, M. B., R. E. Breidenthal, T. W. Choularton, and J. Latham (1984), The effects of turbulent mixing in clouds, *J. Atmos. Sci.*, *41*(2), 299–304, doi:10.1175/1520-0469(1984)041<0299:TEOTMI>2.0.CO;2.

Baumgardner, D., W. Strapp, and J. Dye (1985), Evaluation of the forward scattering spectrometer probe. Part II: Corrections for coincidence and dead-time losses, *J. Atmos. Ocean. Tech.*, *2*(4), 626–632, doi:10.1175/1520-0426(1985)002<0626:EOTFSS>2.0.CO;2.

Baumgardner, D. (1987), Corrections for the Response Times of Particle Measuring Probes, Paper Presented at 6th Symposium on Meteorological Observations and Instrumentation, American Meteorological Society, New Orleans, USA.

Baumgardner, D., and M. Spowart (1990), Evaluation of the forward scattering spectrometer probe. Part III: Time response and laser inhomogeneity limitations, *J. Atmos. Ocean. Tech.*, *7*(5), 666–672, doi:10.1175/1520-0426(1990)007<0666:EOTFSS>2.0.CO;2.

Burnet, F., and J. L. Brenguier (2007), Observational study of the entrainment-mixing process in warm convective clouds, *J. Atmos. Sci.*, *64*(6), 1995-2011, doi:10.1175/JAS3928.1.

Chosson, F., J.-L. Brenguier, and L. Schüller (2007), Entrainment-mixing and radiative transfer simulation in boundary layer clouds, *J. Atmos. Sci.*, *64*(7), 2670–2682, doi:10.1175/JAS3975.1.

Del Genio, A. D., and J. Wu (2010), The role of entrainment in the diurnal cycle of continental convection, *J. Climate*, *23*(10), 2722-2738, doi:10.1175/2009JCLI3340.1.

Devenish, B. J., et al. (2012), Droplet growth in warm turbulent clouds, *Q. J. Roy. Meteor. Soc.*, *138* 1401–1429, doi: 10.1002/qj.1897.

Dye, J., and D. Baumgardner (1984), Evaluation of the forward scattering spectrometer probe. Part I: Electronic and optical studies, *J. Atmos. Ocean. Tech.*, *1*(4), 329–344, doi:10.1175/1520-0426(1984)001<0329:EOTFSS>2.0.CO;2.

Freud, E., D. Rosenfeld, M. O. Andreae, A. A. Costa, and P. Artaxo (2008), Robust relations between CCN and the vertical evolution of cloud drop size distribution in deep convective clouds, *Atmos. Chem. Phys.*, *8*(6), 1661-1675.

Freud, E., D. Rosenfeld, and J. R. Kulkarni (2011), Resolving both entrainment-mixing and number of activated CCN in deep convective clouds, *Atmos. Chem. Phys.*, *11*(24), 12887-12900.

Gerber, H. E., G. M. Frick, J. B. Jensen, and J. G. Hudson (2008), Entrainment, mixing, and microphysics in trade-wind cumulus, *J. Meteorol. Soc. Japan*, *86A* 87–106.

Grabowski, W. W. (2006), Indirect impact of atmospheric aerosols in idealized simulations of convective-radiative quasi equilibrium, *J. Climate*, *19*(18), 4664–4682, doi:10.1175/JCLI3857.1.

Haman, K. E., S. P. Malinowski, M. J. Kurowski, H. Gerber, and J.-L. Brenguier (2007), Small scale mixing processes at the top of a marine stratocumulus—A case study, *Q. J. Roy. Meteor. Soc.*, *133*(622), 213–226, doi:10.1002/qj.5.

Hicks, E., C. Pontikis, and A. Rigaud (1990), Entrainment and mixing processes as related to droplet growth in warm midlatitude and tropical clouds, *J. Atmos. Sci.*, *47*(13), 1589–1618.

Hill, A. A., G. Feingold, and H. Jiang (2009), The influence of entrainment and mixing assumption on aerosol-cloud interactions in marine stratocumulus, *J. Atmos. Sci.*, *66*(5), 1450–1464.

Jeffery, C. A. (2007), Inhomogeneous cloud evaporation, invariance, and Damköhler number, *J. Geophys. Res.*, *112* D24S21, doi:10.1029/2007jd008789.

Jensen, J. B., P. H. Austin, M. B. Baker, and A. M. Blyth (1985), Turbulent mixing, spectral evolution and dynamics in a warm cumulus cloud, *J. Atmos. Sci.*, *42*(2), 173–192, doi:10.1175/1520-0469(1985)042<0173:TMSEAD>2.0.CO;2.

Jensen, J. B., and M. B. Baker (1989), A simple model of droplet spectral evolution during turbulent mixing, *J. Atmos. Sci.*, *46*(18), 2812–2829, doi:10.1175/1520-0469(1989)046<2812:ASMODS>2.0.CO;2.

Kerstein, A. R. (1988), A linear-eddy model of turbulent scalar transport and mixing, *Combust. Sci. Technol.* , *60*(4-6), 391–421.

Kerstein, A. R. (1992), Linear-eddy modelling of turbulent transport. Part 7. Finite-rate chemistry and multi-stream mixing, *J. Fluid Mech.*, *240*(1), 289–313.

Kim, B.-G., M. A. Miller, S. E. Schwartz, Y. Liu, and Q. Min (2008), The role of adiabaticity in the aerosol first indirect effect, *J. Geophys. Res.*, *113*(D5), D05210, doi: 10.1029/2007jd008961.

Krueger, S., C. Su, and P. McMurtry (1997), Modeling entrainment and finescale mixing in cumulus clouds, *J. Atmos. Sci.*, *54* 2697–2712, doi:10.1175/1520-0469(1997)054<2697:MEAFMI>2.0.CO;2.

Krueger, S. K. (2008), Fine-scale modeling of entrainment and mixing of cloudy and clear air, Paper Presented at the 15th International Conference on Clouds and Precipitation, Cancun, Mexico.

Kumar, B., J. Schumacher, and R. Shaw (2012), Cloud microphysical effects of turbulent mixing and entrainment, *Theor Comp Fluid Dyn* 1–16.

Lasher-Trapp, S. G., W. A. Cooper, and A. M. Blyth (2005), Broadening of droplet size distributions from entrainment and mixing in a cumulus cloud, *Q. J. Roy. Meteor. Soc.*, *131*(605), 195–220, doi:10.1256/qj.03.199.

Lehmann, K., H. Siebert, and R. A. Shaw (2009), Homogeneous and inhomogeneous mixing in cumulus clouds: Dependence on local turbulence structure, *J. Atmos. Sci.*, *66* 3641–3659, doi:10.1175/2009JAS3012.1.

Lu, C., Y. Liu, and S. Niu (2011), Examination of turbulent entrainment-mixing mechanisms using a combined approach, *J. Geophys. Res.*, *116* D20207, doi:10.1029/2011JD015944.

Lu, C., Y. Liu, and S. Niu (2013), A method for distinguishing and linking turbulent entrainment mixing and collision-coalescence in stratocumulus clouds, *Chin. Sci. Bull.*, doi:10.1007/s11434-012-5556-6, in press.

Lu, C., Y. Liu, S. Niu, and A. M. Vogelmann (2012a), Observed impacts of vertical velocity on cloud microphysics and implications for aerosol indirect effects, *Geophys. Res. Lett.*, *39*(21), L21808.

Lu, C., Y. Liu, S. Niu, and A. M. Vogelmann (2012b), Lateral entrainment rate in shallow cumuli: Dependence on dry air sources and probability density functions, *Geophys. Res. Lett.*, *39*(20), L20812.

Lu, C., Y. Liu, S. S. Yum, S. Niu, and S. Endo (2012c), A new approach for estimating entrainment rate in cumulus clouds, *Geophys. Res. Lett.*, *39* L04802, doi:10.1029/2011GL050546.

Morrison, H., and W. W. Grabowski (2008), Modeling supersaturation and subgrid-scale mixing with two-moment bulk warm microphysics, *J. Atmos. Sci.*, *65*(3), 792–812, doi:10.1175/2007JAS2374.1.

Paluch, I. R., and D. G. Baumgardner (1989), Entrainment and fine-scale mixing in a continental convective cloud, *J. Atmos. Sci.*, *46*(2), 261–278, doi:10.1175/1520-0469(1989)046<0261:EAFSMI>2.0.CO;2.

Pawlowska, H., J. L. Brenguier, and F. Burnet (2000), Microphysical properties of stratocumulus clouds, *Atmos. Res.*, *55*(1), 15–33.

Raga, G. B., J. B. Jensen, and M. B. Baker (1990), Characteristics of cumulus band clouds off the coast of Hawaii, *J. Atmos. Sci.*, *47*(3), 338–356, doi:10.1175/1520-0469(1990)047<0338:COCBCO>2.0.CO;2.

Rogers, R. R., and M. K. Yau (1989), A Short Course in Cloud Physics, Butterworth Heinemann, Burlington, MA, USA.

Romps, D. M., and Z. Kuang (2010), Nature versus nurture in shallow convection, *J. Atmos. Sci.*, *67*(5), 1655–1666, doi: 10.1175/2009JAS3307.1.

Schlüter, M. H. (2006), The effects of entrainment and mixing processes on the droplet size distributions in cumuli, Master thesis, University of Utah, Salt Lake City, Utah, USA.

Siebert, H., H. Franke, K. Lehmann, R. Maser, E. Wei Saw, D. Schell, R. A. Shaw, and M. Wendisch (2006), Probing finescale dynamics and microphysics of clouds with helicopter-borne measurements, *Bull. Am. Meteorol. Soc.*, *87*(12), 1727–1738, doi:10.1175/BAMS-87-12-1727.

Slawinska, J., W. W. Grabowski, H. Pawlowska, and A. A. Wyszogrodzki (2008), Optical properties of shallow convective clouds diagnosed from a bulk-microphysics large-eddy simulation, *J. Climate*, *21*(7), 1639–1647.

Slawinska, J., W. W. Grabowski, H. Pawlowska, and H. Morrison (2012), Droplet activation and mixing in large-eddy simulation of a shallow cumulus field, *J. Atmos. Sci.*, *69*(2), 444–462.

Su, C.-W., S. K. Krueger, P. A. McMurtry, and P. H. Austin (1998), Linear eddy modeling of droplet spectral evolution during entrainment and mixing in cumulus clouds, *Atmos. Res.*, *47-48* 41–58.

Wyngaard, J. C. (2010), Turbulence in the Atmosphere, Cambridge University Press, New York.

Yum, S. (1998), Cloud droplet spectral broadening in warm clouds: An observational and model study, PhD thesis, University of Nevada, Reno, Nevada, USA.